

We are IntechOpen, the world's leading publisher of Open Access books Built by scientists, for scientists

6,900

Open access books available

186,000

International authors and editors

200M

Downloads

Our authors are among the

154

Countries delivered to

TOP 1%

most cited scientists

12.2%

Contributors from top 500 universities



WEB OF SCIENCE™

Selection of our books indexed in the Book Citation Index
in Web of Science™ Core Collection (BKCI)

Interested in publishing with us?
Contact book.department@intechopen.com

Numbers displayed above are based on latest data collected.
For more information visit www.intechopen.com



Hydrometallurgical Recovery Process of Rare Earth Elements from Waste: Main Application of Acid Leaching with Devised τ -T Diagram

Namil Um

Additional information is available at the end of the chapter

<http://dx.doi.org/10.5772/intechopen.68302>

Abstract

Rare earth elements (REEs) are essential ingredients for developing modern industry as well as designing and developing high technology products used in our daily lives. However, China monopolizes the supply chain for rare metals, and there have been growing concerns around limited supply in other countries. As such, there is demand for intensive research into the recovery of REEs from a large amount of the wastes produced in various industry links, including radioactive residues, polishing powders, catalysts, magnetic materials, batteries, etc., because they can play an important role in the resource supply. Therefore, in this chapter, we introduced the main application of acid-leaching process as a hydrometallurgical method to obtain the REEs from waste containing rare earths; the effective application of acid-leaching process is discussed through the leaching behavior of rare earths in acidic solution and the synthesis method of target rare earth during acid leaching for purifying it from non-rare earth. The devised $\tau - T$ diagram application to the hydrometallurgical method for selective acid leaching is also discussed using the leaching kinetics of rare earth in acidic solution and might be helpful to further corroborate the future plans for technical scale with recovery effectiveness of REEs.

Keywords: rare earth element, hydrometallurgical recovery process, acid leaching, leaching kinetics, devised $\tau - T$ diagram

1. Introduction

Many industries have become highly dependent on products that cannot be made without using rare earth metals. Although the importance of REEs is increasing, the supply and the price are not stable [1, 2]. For that reason, many trading corporations and manufacturers globally have been aware of the importance of REEs for the industrial economy and have been planning their

strategies to secure a stable supply. As such, there is demand for intensive investigation into the recovery of rare earths from various types of wastes containing rare earth elements (REEs) as they should serve as a new source and can play a leading role in securing resources [3–5].

Indeed, a large amount of wastes containing REEs have been produced in various industry links, including disused hydrogen storage batteries, magnetic materials, rare metal catalysts, polishing powders, hydrometallurgy residues, rare metal radioactive residues, etc. Therefore, many researchers are beginning to take an interest in the recovery of REEs by chemical and physical methods [6–8].

In general, the pyrometallurgical and hydrometallurgical processes have been used by many researchers and other professionals in the field of the recovery of material of interest from various types of mineral. The main disadvantages of pyrometallurgical process are the severe corrosion problems (generation of dust and gas) and their high energy requirements, whereas the hydrometallurgical process is more environmentally suitable and economical to treat the target materials on a small scale [9, 10].

The leaching process with acidic solution, which is one of the hydrometallurgical processes including leaching, solvent extraction, ion exchange and precipitation, has some drawbacks in terms of the separation and recovery of materials of interest from undesired species, because another method after the leaching process is needed to separate the materials of interest. Nevertheless, the leaching process is simple, and its cost is not expensive to implement for the treatment of the target materials. Another reason for this is discussed in more detail in Section 3.

Therefore, in this chapter, we will introduce the main application of the leaching process among the hydrometallurgical processes, as methods to improve or to help the effective recovery of REEs from waste. In addition, the possibility of the selective leaching method with the devised $\tau - T$ diagram is also discussed using the characteristics of leaching kinetics of rare earth oxides (REOs) on acid leaching.

2. Hydrometallurgical process for recovery of rare earth elements (REEs) from waste

Hydrometallurgical operation is an essential part of extractive metallurgy and utilized in various metal refining plants throughout the world. This is known to be a flexible, highly selective and environmentally friendly method for the treatment of raw materials. The principal processes employed during hydrometallurgical treatment of the resources mainly include leaching, solvent extraction, ion exchange and precipitation, which varies depending on the material of interest to be recovered. The basic processes used for REEs recovery from the waste are similar to hydrometallurgical methods.

2.1. Leaching

Leaching REEs from the waste is an important part of rare earth processing using hydrometallurgical route. Physically beneficiated concentrates are leached in a suitable lixiviant directly

or after heat treatment to dissolve the metallic elements. The known processes range from acid leaching with H_2SO_4 , HCl , HNO_3 to leaching with $NaCl$ or $(NH_4)_2SO_4$ of ion adsorbed clays. Complete understanding of these processes is essential for applying them to develop more feasible methods for the recovery of REEs from the waste. Therefore, this chapter focuses primarily on the main application of the acid-leaching process as a hydrometallurgical method needed in order to recovery REEs from waste containing rare earths.

2.2. Solvent extraction

Solvent extraction is an important technique that can usually be employed to separate and extract individual rare earths to get their mixed solutions and compounds from leached solutions after the leaching process using different cationic, anionic and solvating extractants viz. D2EHPA, Cyanex 272, PC 88A, Versatic 10, TBP, Aliquat 336, etc. For example, D2EHPA is the most widely studied extractant for rare earth separation from nitrate, sulfate, chloride and perchlorate solutions. Saponified PC 88A has been reported for their separation from chloride solutions while tributyl phosphate (TBP), a solvating extractant that extracts their nitrates from the aqueous solutions.

2.3. Ion exchange and precipitation

During the ion exchange process, different ion exchange cationic or anionic resins are employed depending on the constituent of the aqueous solution using batch or continuous mode in column to extract rare earths from leached solutions with low rare earth concentration. Cation exchange can be primarily used to obtain REEs. The affinity of the exchanged ions for the cation exchanger depends majorly on the charge, size and degree of hydration of the exchanged ions. However, the mechanism of the processes involved in anion exchangers was much more complex and could not be explained clearly. REEs show little tendency to form anionic complexes with simple inorganic ligands.

3. Why acid leaching?

REEs have strong affinity for oxygen, and thus, their resources are principally present in oxidic form as REOs. In addition, the crystal structure of REOs has its own peculiarities such as polishing ability, mechanical strength, wear resistance, etc. Thus, the rare earth as oxides is increasingly establishing themselves, with unique applications in numerous fields, such as the catalysts, ceramics, phosphores, glass and polishing, as shown in **Table 1** [11]. After being used for numerous applications in various fields, a large amount of waste containing REOs is generated. And even when the waste with nonoxides of REEs is generated, the initial step with a calcinations process for hydrometallurgical recovery process, which does not liberate the material interest from host waste, is available to oxidize the REEs; when the waste is treated using a high temperature of at least $500^\circ C$, the REEs in remaining residue will be oxidized to REOs. Assuming that all REEs exist as an oxide, the leaching behavior of REOs in an acid solution will be the key for effective recovery of REEs.

Application	RE technology	Required RE	Materials	Consumption (%)
Catalysts	Petroleum refining, catalytic converter, diesel additives, chemical processing, industrial pollution scrubber	La, Ce, Pr, Nd	REOs	19
Ceramics	Capacitors, sensors, colorants, scintillators, refractories	La, Ce, Pr, Nd, Y, Eu, Gd, Bu, Dy	REOs, LaCl ₃ : Ce, Eu: (Y, Gd) ₂ O ₃ , Pr, Ce: Gd ₂ O ₂ S	6
Magnets	Disc drives, MRI, power generation, microphones and speakers, magnetic refrigeration	Nd, Pr, Tb, Dy	Alloys, e.g., SmCo ₅ , Nd ₂ Fe ₁₄ B, Tb _x Dy _{1-x} Fe ₂ (x~0.3)	21
Metallurgical alloys	NiMH batteries, fuel cells, steel, lighter flints, superalloys, aluminum/magnesium	La, Ce, Pr, Nd, Y	Intermetallics, e.g., Lm (Ni _{3.6} Mn _{0.4} Al _{0.3}), CeCoLn ₅ , YBa ₂ Cu ₃ O ₇	18
Phosphores	Display phosphors (CRT, LPD, LCD), fluorescent lighting, medical imaging, lasers, fiber optics	Eu, Y, Tb, Nd, Er, Gd, Ce, Pr	REOs, dopants, e.g., Ce ₂ O ₅ S: Tb ³⁺ , SrGa ₂ S ₄ : Eu ²⁺ , Tb: YAG, Tb: (La,Ca)PO ₄	7
Glass and polishing	Polishing compounds, decolorisers/colorisers, UV resistant glass, X-ray imaging	Ce, La, Pr, Nd, Gd, Er, Ho	REOs	22
Others	Nuclear, pigments	Eu, Gd, Ce, Y, Sm, Er, Ce, Y	Gd ₂ O ₃ , Er ₂ O ₃ , EuB ₆ , CeH ₂ , YH ₃ , Y ₂ O ₃ , CeO ₂	7

Table 1. Applications of RE metals (Kim and Osseo-Asare, 2012) [11].

In terms of the cost consumption, the main advantages of the acid leaching process include lower capital (e.g., no expensive equipment and cheaper materials of construction) and lower operating costs (e.g., lower energy requirement and less maintenance). In addition, it is possible to apply other methods during acid leaching for purification of the material of interest (the reason for this is discussed in more detail in Section 4.2), and, the possibility for the selective leaching of REEs, using the characteristic of leaching kinetics, can be confirmed (the reason for selective leaching of REEs is discussed in more detail in Sections 5.2 and 5.3).

4. Acid leaching process for recovery of rare earth

4.1. Leaching behavior of rare earth oxides (REOs) on acid leaching

Cerium oxide with in a tetravalent state is the most stable phase among the rare earth oxides, so there are many difficulties associated with dissolving it in acidic solutions. For example, the E-pH diagram for Ce-H₂O system shown in **Figure 1a** indicates that the pH required for dissolution to Ce⁴⁺ from cerium oxide is in the range of < -0.8 at atmospheric pressure [12].

Therefore, the cerium oxide can be dissolved in highly concentrated acid solutions and at elevated temperatures. For confirmation of cerium oxide dissolution in sulfuric acid solution, two chemical reactions are considered to be involved in the conversion of cerium oxide into

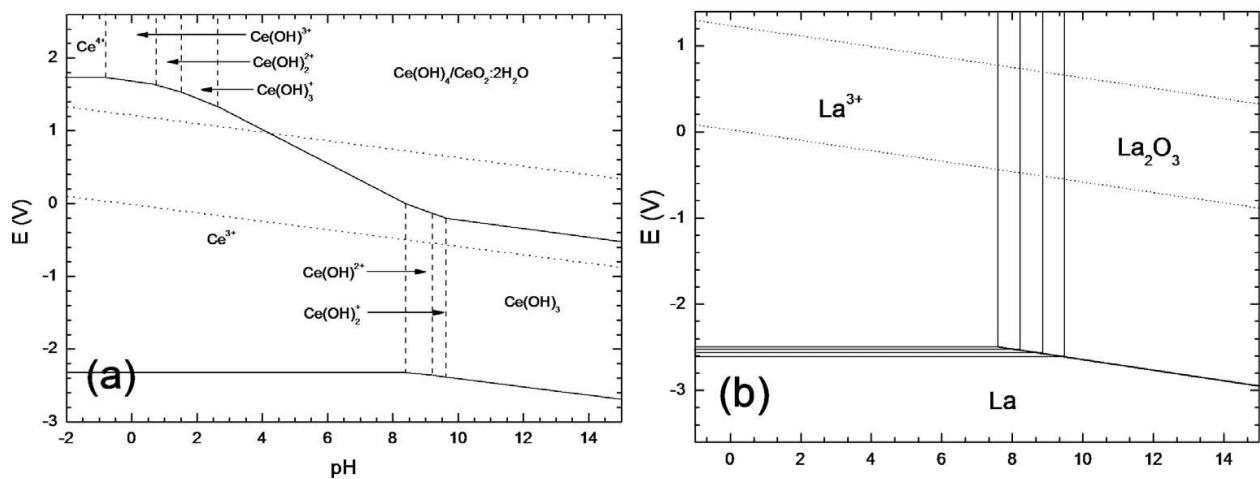


Figure 1. (a) An updated Pourbaix diagram for cerium in aqueous perchlorate and (b) lanthanum in water (Scott et al., 2002) [12].

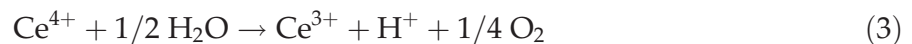
cerium sulfate in H₂SO₄-H₂O solution as follows. Cerium oxide reacts with sulfuric acid at atmospheric pressure according to the following dissolution reaction.



At high sulfuric acid concentrations, the concentration of mixed cerium exceeds its solubility at an early stage. Then, cerium cations dissolved under saturated conditions directly form cerium sulfate as follows:



Cerium (IV) cations can be reduced to cerium (III) cations as follows.



However, it can be estimated that this reaction proceeds much less than the cerium sulfate formation according to the following experimental results shown in **Figure 2a**. This result summarized by Um and Hirato (2012) [13] showed that it took more than 48 hours to completely dissolve 0.02 mol CeO₂ powder with 2.5 μm average particle size in 100 ml of sulfuric acid (8 mol/dm³) at 125°C. Comparing the XRD patterns of the precipitate (mixture of Ce-oxide and sulfate) provide evidence for the conversion of cerium oxide into cerium sulfate clearly (**Figure 2b**) and also support the results shown in **Figure 2a**; the intensity of the diffraction peaks originating from cerium sulfate increased with an increase in reaction time, while that from cerium oxide decreased.

Unlike cerium oxide, the dissolution of other REOs presenting as trivalent state occurred rapidly; for example, the E-pH diagram for lanthanum-water system shown in **Figure 1b** indicates that the pH required for dissolution to La³⁺ from lanthanum oxide is in the range of > at least 7.5 according to La₂O₃ + 6H⁺ → La³⁺ + 3H₂O. In addition, the results summarized by Um and Hirato (2013) [14] show that the dissolution of La, Pr, and Nd oxides took less than

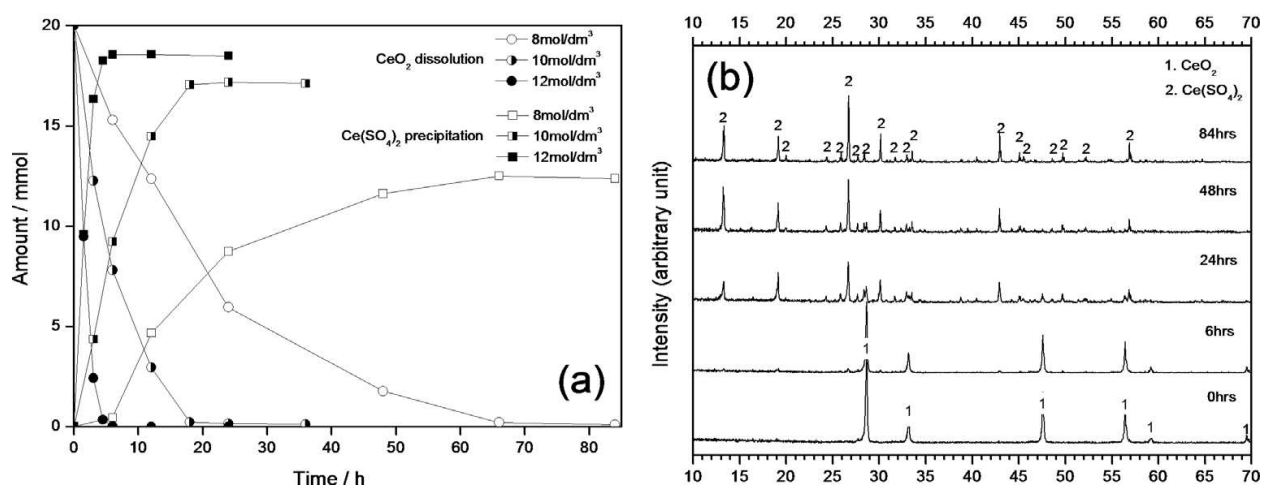


Figure 2. (a) Effect of sulfuric acid concentration on conversion kinetics of cerium oxide into cerium sulfate in acidic solution and (b) XRD patterns of the precipitate obtained at different reaction times (Um and Hirato, 2012) [13].

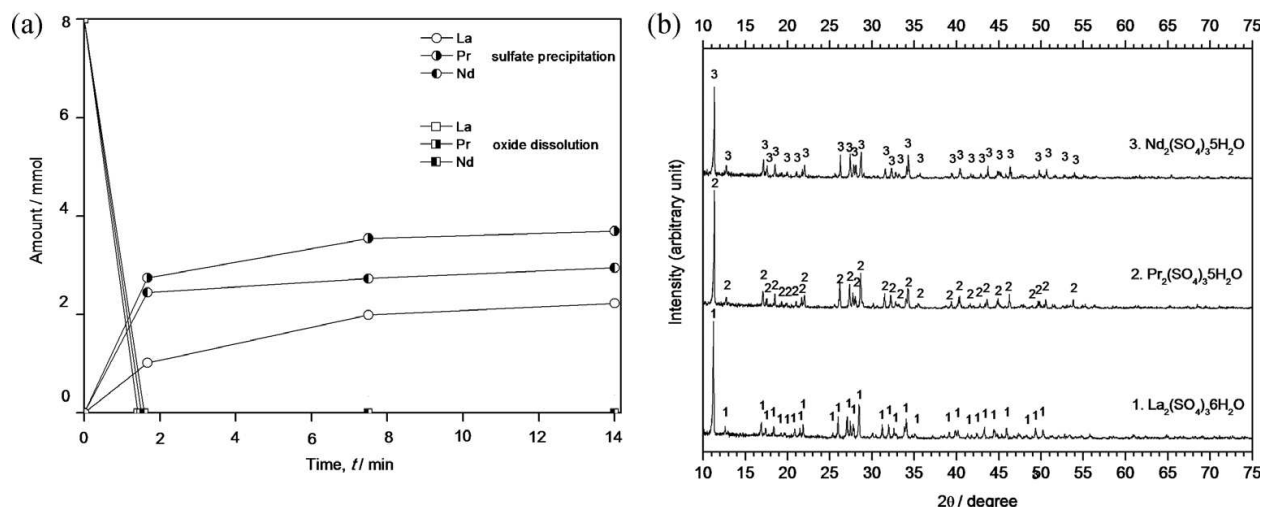
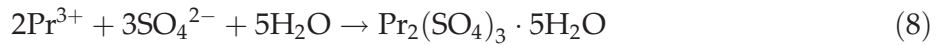


Figure 3. (a) Conversion kinetics of La_2O_3 , Pr_2O_3 , and Nd_2O_3 into La, Pr, and Nd sulfates in sulfuric acid solutions and (b) XRD patterns of La, Pr, and Nd sulfates obtained after 14-minute conversion kinetics (Um and Hirato, 2013) [14].

1 minute to dissolve in acid solution shown in **Figure 3a**. Under high initial amount of La_2O_3 , Pr_2O_3 , and Nd_2O_3 per sulfuric acid solutions, the concentration of dissolved La^{3+} , Nd^{3+} , and Pr^{3+} exceeds the solubility and these cations directly form sulfate. The results of the XRD patterns shown in **Figure 3b** provide evidence for that conversion. The chemical reactions below [Eqs. (4)–(9)] are considered to be involved in the conversion of La, Pr, and Nd oxides into precipitated sulfate in sulfuric acid solutions:





4.2. Synthesis method for purification of rare earth during acid leaching

As mentioned in Section 1, the leaching process using an acidic solution for the recovery of rare earth from the waste has its demerits with respect to separation and recovery. The materials of interest are dissolved along with undesired species in the solution, and another method is thus needed to separate these materials; if waste containing REEs is dissolved in acid solutions, difficulties in purifying REEs from non-rare earth ions inevitably arise. Therefore, the synthesis method for purification of REEs during acid leaching is one of the simpler separation methods. According to Um and Hirato (2012 and 2016) [15, 16], for purification of target rare earth from rare earth polishing powder wastes, the REEs can be precipitated in the form of rare earths and sodium double sulfate ($\text{NaRe}(\text{SO}_4)_2 \cdot x\text{H}_2\text{O}$) through the addition of Na_2SO_4 to $\text{H}_2\text{SO}_4\text{-H}_2\text{O}$ solutions during the acid leaching because $\text{NaRe}(\text{SO}_4)_2 \cdot x\text{H}_2\text{O}$ is poorly soluble under acidic conditions.

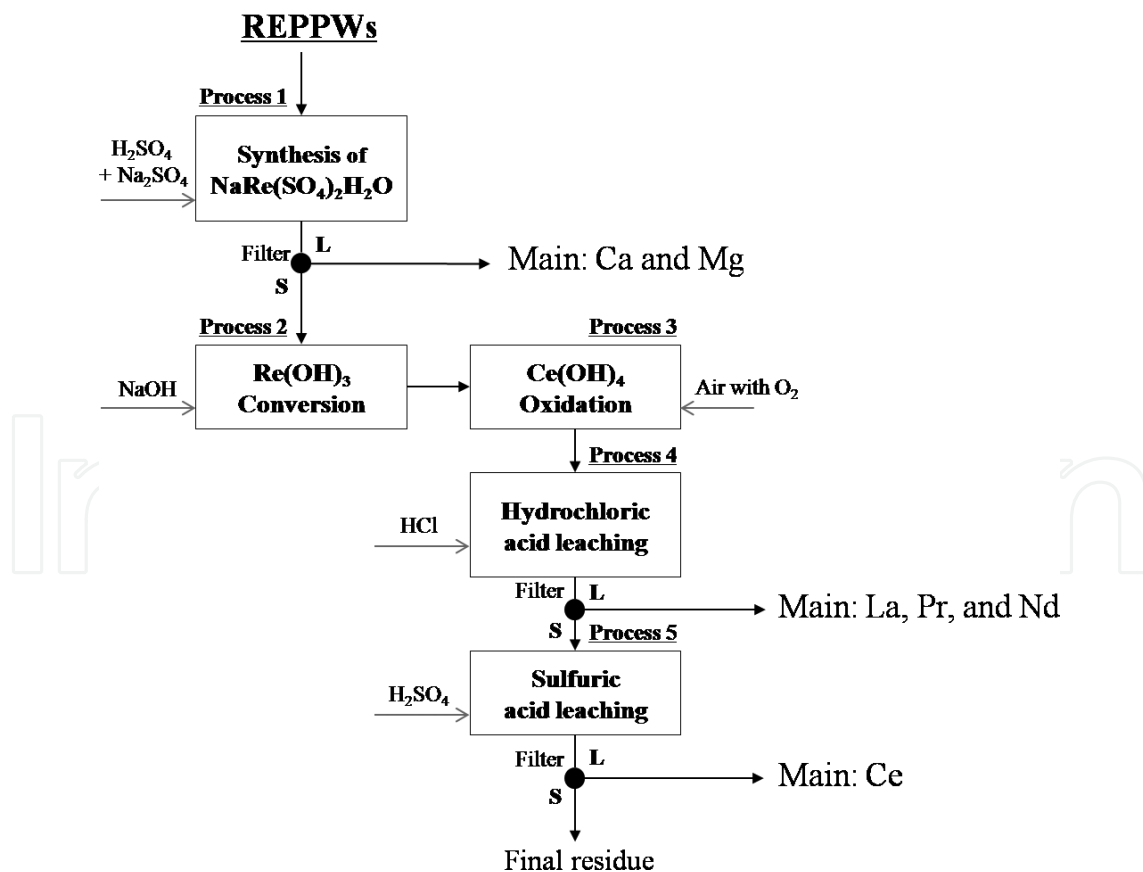


Figure 4. Schematic flow diagram for separation of rare earth elements from rare earth polishing powder wastes via a devised hydrometallurgical process (Um and Hirato, 2016) [16].

A five-process strategy for separation of REEs from polishing powder wastes in **Figure 4** was employed in the result from Um and Hitato (2016) [16]: process 1, the high yield of synthesized $\text{NaRe}(\text{SO}_4)_2 \cdot x\text{H}_2\text{O}$ from REOs in $\text{Na}_2\text{SO}_4\text{-H}_2\text{SO}_4\text{-H}_2\text{O}$ would be controlled by the function of the reaction temperature, sulfuric acid concentration, and Na_2SO_4 concentration; process 2, $\text{NaRe}(\text{SO}_4)_2 \cdot \text{H}_2\text{O}$ is converted into $\text{Re}(\text{OH})_3$ using sodium hydroxide (NaOH) solution; process 3, the oxidation of $\text{Ce}(\text{OH})_3$ to $\text{Ce}(\text{OH})_4$ via the injection of air including O_2 would be advantageous for the separation of cerium, existing as the main phase in polishing powder wastes, from other rare earths; process 4, the acid leaching with hydrogen chloride (HCl) at 25°C should be limited until the pH value is between 2.5 and 3.5 because a high yield of rare earths, except cerium, is obtained after acid leaching; process 5, the residue after process 4 is added to acid solution with H_2SO_4 to separate cerium from the final impurities. As shown in **Figure 4**, this result suggests the possibility of target lanthanide element from the other REEs using selective synthesis method. The separation of cerium from the other REEs can be carried out by selective synthesis of the tetravalent Ce-hydroxide in process 3, because the trivalent ceric ions, which is the major phase in polishing powder wastes, is the most likely to be oxidize to its tetravalent state by bubbling air with oxygen, unlike the other REEs presenting as trivalent cations.

5. Leaching kinetics and application of devised $\tau - T$ diagram

5.1. Leaching kinetics

The experimental data of REOs dissolution, which was performed under various conditions of acid concentration, reaction temperature, solid-to-liquid ratio, particle size, etc., were made to fit the shrinking core model to REO-dissolution vs. time curves, as follows.

The dissolution mechanism of B (solid) into A (acid-liquid) is described as a two-step process; the first step is B dissolution into A, and the second step is that the B cations dissolved under saturated conditions directly form B-precipitate in an aqueous acid medium, as mentioned in Section 4.1. Because these steps occur consecutively, if one is slower than the other, the step becomes rate determining. The formation of B-precipitate under saturated conditions is dependent on the acid concentration, the reaction temperature, etc., and its rate is much faster than the dissolution rate. Therefore, assuming that this reaction does not affect the dissolution rate, the rate of the leaching reaction between the B solid and the A liquid becomes the rate-determining step:



According to Wadsworth and Miller (1979) [17], Liquid-solid reaction kinetics of dense (nonporous) particles is described by the most widespread shrinking core model. In the liquid-solid heterogeneous system, the reaction rate may be controlled as certain individual steps such as diffusion through the fluid film, product layer diffusion control, and surface chemical reaction. The experimental data of REOs dissolution, which was performed under various conditions of reaction temperature, acid concentration of the liquid, solid-to-liquid ratio, and particle size, were made to fit the shrinking core model with surface chemical

reaction to REOs-dissolution vs. time curves according to Um and Hirato (2012 and 2013) [13, 14]. This result shows evidence of the leaching kinetics of REOs to fit the shrinking core model, which is discussed in detail below.

If the leaching reaction between the B solid and the A acid-liquid becomes the rate-determining step so that the reaction is followed by the shrinking core model with surface chemical reaction as shown in **Figure 5**, the rate of disappearance of B ($-r_B$; mol/m²h) can be described as follows:

$$-r_B = \frac{1}{S_t} \frac{dN_B}{dt} \quad (11)$$

S_t (m²) denotes the surface area of the B; dN_B (mol), the amount of B disappearing; in particular, if $dN_B \rightarrow bdN_A$ (disappearing acid concentration of A; mol) according to the chemical reaction and their stoichiometric coefficient in Eq. (10), it is possible to obtain the expression with k_1 and C_A :

$$-\frac{1}{4\pi r^2} \frac{dN_B}{dt} = -\frac{b}{4\pi r^2} \frac{dN_A}{dt} = bk_1 C_A \quad (12)$$

Here, k_1 (h⁻¹) is the rate constant of first-order reaction controlled by the interaction between the A and the surface of B, and C_A (mol/m²) is the concentration of A existing on the surface of B. Also, the amount of B disappearing can be expressed using the density and the volume of B as follows:

$$dN_B = \rho dV_t = \rho \cdot d\left(\frac{4}{3}\pi r^3\right) = \rho 4\pi r^2 dr \quad (13)$$

ρ (mol/m³) presents the density of B; V_t (m³), the volume of B (solid) after dissolution time t ; r (m), the radius size of B after dissolution time t . According to Eqs. (12) and (13), Eqs. (14) and (15) can be written as:

$$-\frac{1}{4\pi r^2} \rho 4\pi r^2 \frac{dr}{dt} = -\rho \frac{dr}{dt} = bk_1 C_A \quad (14)$$

and

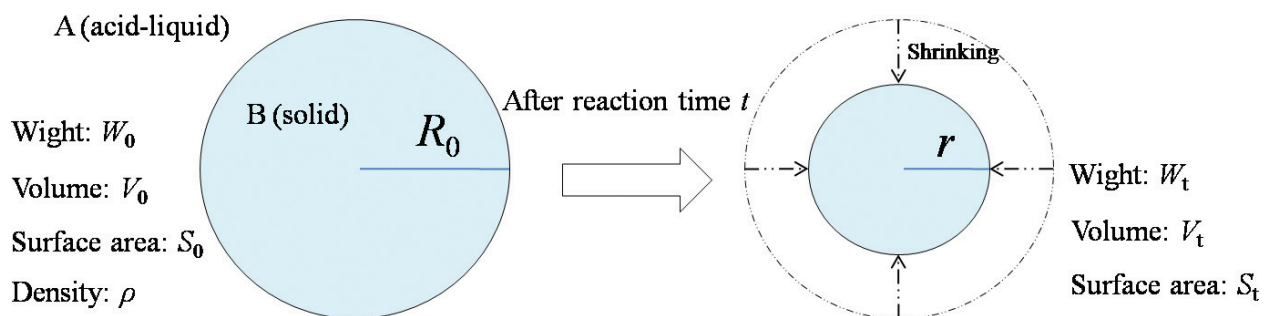


Figure 5. Shrinking core model with surface chemical reaction between A (acid-liquid) and B (solid).

$$\rho \int_R^r dr = bk_1 C_A \int_0^t dt \quad (15)$$

Integrating, yield the following expression for time t :

$$t = \frac{\rho}{bk_1 C_A} (R_0 - r) \quad (16)$$

If $r=0$, the time for complete dissolution reaction (τ ; h) can be expressed as:

$$\tau = \frac{\rho R_0}{bk_1 C_A} \quad (17)$$

Combining these two Eqs. (16) and (17) in the form with the radius sizes of B before and after dissolution time ($\frac{r}{R_0}$) gives the expression for $\frac{t}{\tau}$ and k (apparent rate constant; h^{-1}):

$$\frac{t}{\tau} = 1 - \frac{r}{R_0} \quad (18)$$

and

$$k = \frac{1}{\tau} = \frac{bk_1 C_A}{\rho R_0} \quad (19)$$

For calculating k , it is necessary to confirm the change of the radius size of B before and after dissolution time. However, it is not easy to measure the size of target particle because of their heterogeneous spherical shape. Therefore, Eq. (20) can lead to advanced means of obtaining much easier measurement with the weight of B rather than that with the radius size.

$$\frac{W_t}{W_0} = \frac{\frac{W_t}{\rho}}{\frac{W_0}{\rho}} = \frac{V_t}{V_0} = \frac{\frac{4}{3}\pi r^3}{\frac{4}{3}\pi R_0^3} = \left(\frac{r}{R_0}\right)^3 \quad (20)$$

Here, W_0 and W_t represent the initial and residual amount of B vs. dissolution time t , respectively. X_t represents the dissolved fraction vs. dissolution time t , which was then calculated as follows:

$$X_t = 1 - \frac{W_t}{W_0} \quad (21)$$

Combining these Eqs. (18)–(21), the rate equation of surface chemical reaction controlled process for heterogeneous spherical particles of B is established as follows:

$$kt = 1 - (1 - X_t)^{\frac{1}{3}} \quad (22)$$

The rate constant k varies with experimental conditions and is the function of reaction temperature, acid concentration, particle size, and initial amount of B (target REEs) per A (acid-liquid) (B/A). When B is dissolved into acid-liquid in all experiments, with the dissolution rate constant, considered as the function of reaction temperature, sulfuric acid concentration, particle size, and B/A, can be expressed by the following equation:

$$k = k_0' e^{-E_a/RT} C^m p^n S^l \quad (23)$$

where E_a is the activation energy (kJ/mol); R , the ideal gas constant, 8.314×10^{-3} (kJ/molK); T , the reaction temperature (K); C , sulfuric acid concentration (mol/dm³); p , particle size (μm); S , B/A (mol/dm³); k_0' , pre-exponential factor; and m , n , and l are constants.

It can be seen that $1 - (1 - X_t)^{\frac{1}{3}}$ and time t are in a linear relationship and the slope of these line is k according to Eq. (22). In addition, the $\ln k$ values calculated from these k values were plotted against $1/T$, $\ln C$, $\ln p$, and $\ln S$ using equations $k = k_1' e^{-E_a/RT}$ (relationship between rate constant and activation energy with reaction temperature), $k = k_2' C^m$ (rate constant and acid concentration constant), $k = k_3' p^n$ (rate constant and particle size constant), and $k = k_4' S^l$ (rate constant and B/A constant) according to Eq. (23) where k_1' , k_2' , k_3' , and k_4' are the pre-exponential factors. It can also be seen that $\ln k$ and $1/T$ (or $\ln C$, $\ln p$, and $\ln S$) are in a linear relationship and the slope of this line is $-E_a/RT$ (or m , n , and l).

The experimental data obtained from the study of Um (2012) [18], which shows the effect of reaction temperature, sulfuric acid concentration, initial amount of cerium oxide per sulfuric acid solutions (B/A), and particle size on the conversion kinetics of cerium oxide in sulfuric acid solutions, were fitted with theoretical functions derived from Eqs. (22) and (23). **Figure 6a** shows the effect of reaction temperature on the dissolution rate of cerium oxide. Such results indicate that $1 - (1 - X_t)^{\frac{1}{3}}$ and time t are in a linear relationship; the rate constants are calculated as slopes of the straight lines. The rate constants were used to determine the Arrhenius plot between $\ln k$ and $1/T$ (application of $k = k_1' e^{-E_a/RT}$) in **Figure 6b**. As shown in **Figure 6b**, the increase in dissolution rate constant with increasing temperature obeyed the Arrhenius equation with an activation energy of 123kJ/mol. The results for the effect of sulfuric acid concentration were applied to the kinetic model and rate constants for various sulfuric acid concentrations (8, 10, and 12 mol/dm³) were determined by using the linear regressions in **Figure 6c**. A plot of $\ln k$ versus $\ln C$ in **Figure 6d** shows that the constant m was calculated to be 6.54. This large constant indicates a strong effect of acid concentration on the dissolution rate. The slopes in **Figure 6e** determined the rate constant related to the particle sizes (2.5, 10.0, 47.5, and 112.5 μm). As seen in **Figure 6e**, the decrease in particle size increased the dissolution rate of cerium oxide. The plot of $\ln k$ versus $\ln p$ in **Figure 6f** shows that the constant n was calculated to be -0.78 . In addition, the linear regressions in **Figure 6g** were used to calculate the reaction rate constants for various C/S (0.04, 0.12, and 0.2 mol/dm³). And the plot of $\ln k$ versus $\ln S$ in **Figure 6h** shows that the constant l was calculated to be -0.03 , indicating that C/S has no effect on the dissolution rate of cerium oxide. Therefore, the kinetics equation on the dissolution of cerium oxide in sulfuric acid solution was $k = 3.26 \times 10^8 e^{-14800/T} C^{6.54} p^{-0.78} S^{-0.03}$.

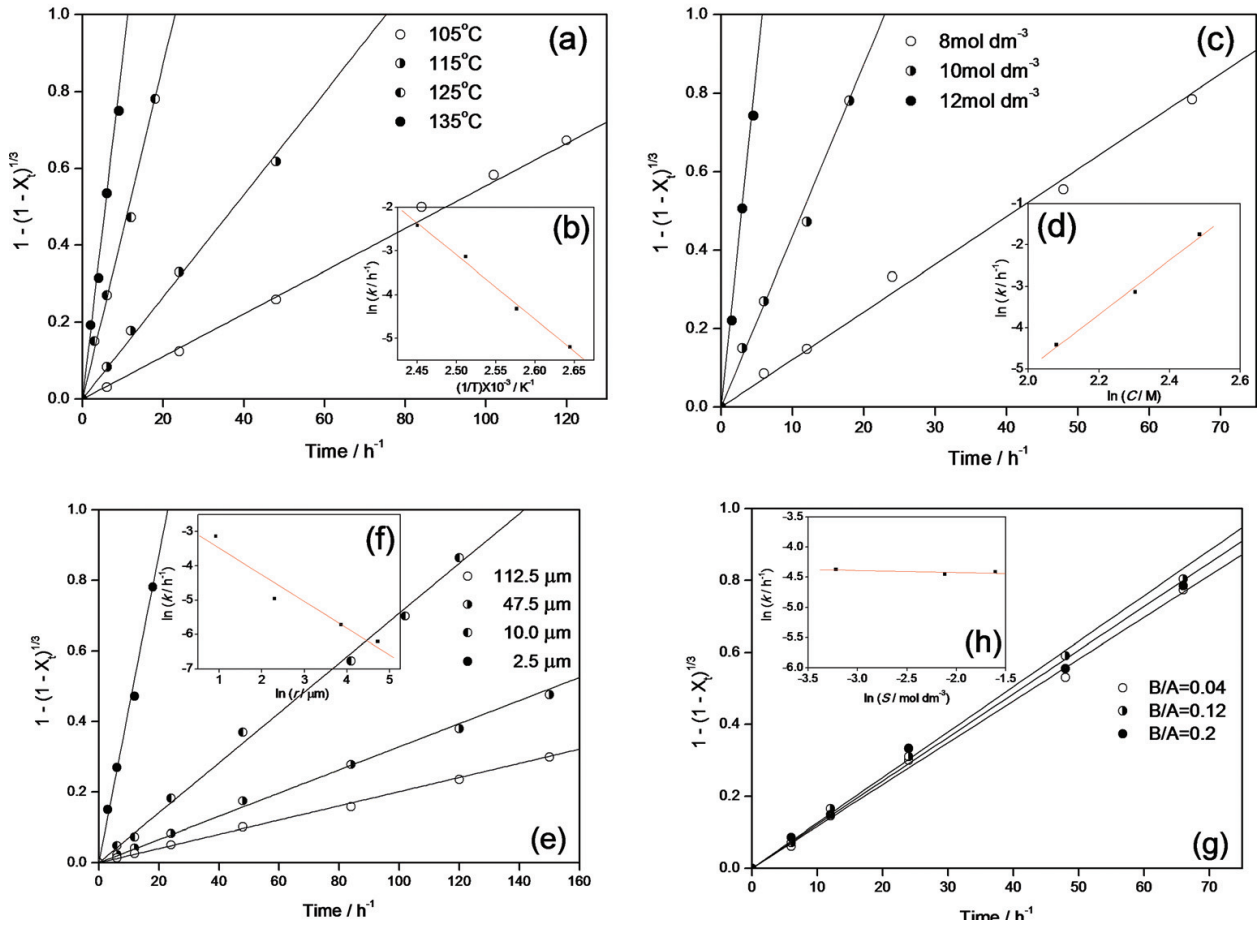


Figure 6. Plots of $1 - (1 - X_t)^{1/3}$ versus reaction time for (a) reaction temperatures, (c) different sulfuric acid concentrations, (e) particle sizes, and (g) B/A, and effect of (b) reaction temperature, (d) sulfuric acid concentration, (f) particle size, and (h) B/A on the conversion rate constants (Um, 2012) [18].

5.2. Devised $\tau - T$ diagram

The relationship between the time for complete dissolution reaction (τ) and the reaction temperature (T) will be the effective methods in terms of separation and recovery of REEs from the waste during the leaching process. In the case of a REOs- H_2SO_4 - H_2O system, the relationship between τ and T can be constructed using the kinetics equation relating to the rate constant k with various functions of reaction temperature, sulfuric acid concentration, particle size, initial amount of REOs per acid solution, etc. If this relationship is dependent on the acid concentration, which affects the dissolution rate between the undesired species and the materials of interest (REOs), as well as the reaction temperature, the relationship can be devised using the equation of $k = k'_5 e^{-E_a/RT} C^m$ (k'_5 ; the pre-exponential factor) obtained from Eq. (23).

Rearranging the equation of $k = k'_5 e^{-E_a/RT} C^m$, one obtains:

$$\ln k = -\left(\frac{E_a}{R}\right) \frac{1}{T} + (\ln k'_5 + m \ln C) \quad (24)$$

The equation shows that $\ln k$ and $1/T$ have a linear relationship, and the slope of this line is $-\left(\frac{E_a}{R}\right)$. Putting the activation energies of the undesired species ($E_{a_{us}}$) and material of interest

($E_{a_{int}}$) and the acid concentration constants of the undesired species (m_{us}) and material of interest (m_{int}) into the Eq. (24) respectively, the expressions between $\ln k$ and $1/T$ can be obtained as follows:

$$\text{Undesired species : } \ln k = -\left(\frac{E_{a_{us}}}{R}\right) \frac{1}{T} + (\ln k'_5 + m_{us} \ln C) \quad (25)$$

and

$$\text{Material of interest : } \ln k = -\left(\frac{E_{a_{int}}}{R}\right) \frac{1}{T} + (\ln k'_5 + m_{int} \ln C) \quad (26)$$

Converting $\ln k$ into the time for complete dissolution reaction ($\tau = e^{-\ln k}$) according to Eq. (19), devised $\tau - T$ diagrams can be obtained as follows:

$$\text{Undesired species : } \tau = e^{\left[\left(\frac{E_{a_{us}}}{R}\right) \frac{1}{T} - (\ln k'_5 + m_{us} \ln C)\right]} \quad (27)$$

and

$$\text{Material of interest : } \tau = e^{\left[\left(\frac{E_{a_{int}}}{R}\right) \frac{1}{T} + (\ln k'_5 + m_{int} \ln C)\right]} \quad (28)$$

Two types of $\tau - T$ diagram can be explained as shown in **Figure 7**.

In Type 1, the linear relation between $\ln k$ and $1/T$ of undesired species [Eq. (25)] lies with that of material of interest [Eq. (26)] over the whole range of $1/T$; the $\ln k$ values of Y-axis are converted into τ , whereas Type 2 shows that the exponential function related to τ and $1/T$ of Eqs. (27) and (28) is placed over the range considered. As shown in **Figure 7**, the increasing difference in τ between two linear relations (or exponential function curves) in the $\tau - T$ diagram can lead the material of interest to be separated from the undesired species by leaching.

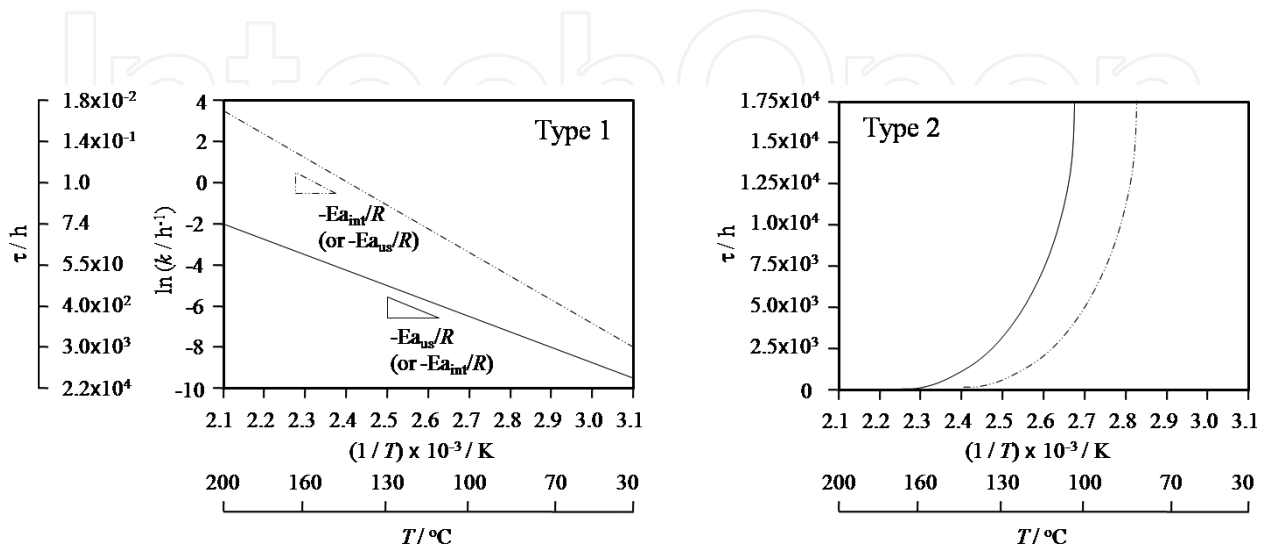


Figure 7. Two different types of $\tau - T$ diagrams.

From the point of view of the linear relation, the various cases of the relationship between the undesired species and the material of interest in the devised $\tau - T$ diagram of Type 1 can be expected as follows:

Case 1: $E_{a_{int}} \neq E_{a_{us}}$ and $m_{us} \doteq m_{int}$

Case 2: $E_{a_{int}} \neq E_{a_{us}}$ and $m_{int} \neq m_{us}$

Case 2-1: ($E_{a_{int}} > E_{a_{us}}$ and $m_{int} > m_{us}$) or ($E_{a_{int}} < E_{a_{us}}$ and $m_{int} < m_{us}$)

Case 2-2: ($E_{a_{int}} < E_{a_{us}}$ and $m_{int} > m_{us}$) or ($E_{a_{int}} > E_{a_{us}}$ and $m_{int} < m_{us}$)

Case 3: $E_{a_{int}} \doteq E_{a_{us}}$ and $m_{int} \neq m_{us}$

Case 4: $E_{a_{int}} \doteq E_{a_{us}}$ and $m_{us} \doteq m_{int}$

Because the difference in the activation energies as the slope of the linear relation in Eqs. (25) and (26) makes two lines angle inward toward the center, the difference in τ is definitely distinctive as the reaction temperature changes. For example, in Case 1, the difference in τ decreases with increasing reaction temperature, while, in Case 2-1, it increases. In Case 2-2, the wide difference between two materials can be observed over the whole range of temperature (T). If there is very little difference in the activation energies ($E_{a_{int}} \doteq E_{a_{us}}$), it is implied that the lines are nearly parallel with a given separation, as shown in Case 3 and Case 4; especially, in Case 4, the separation of the material of interest from the undesired species is difficult in terms of separation and recovery due to the similarity of the two lines (**Figure 8**).

The results from Um and Hirato (2013) [14] showing kinetics data of CeO_2 and Al_2O_3 dissolution performed under various conditions of sulfuric acid concentration and reaction temperature indicate that the $\tau - T$ diagram in $\text{CeO}_2\text{-Al}_2\text{O}_3\text{-H}_2\text{SO}_4\text{-H}_2\text{O}$ system could be a good example of Case 3. As for the dissolutions of CeO_2 and Al_2O_3 , the following equations were obtained as follows:

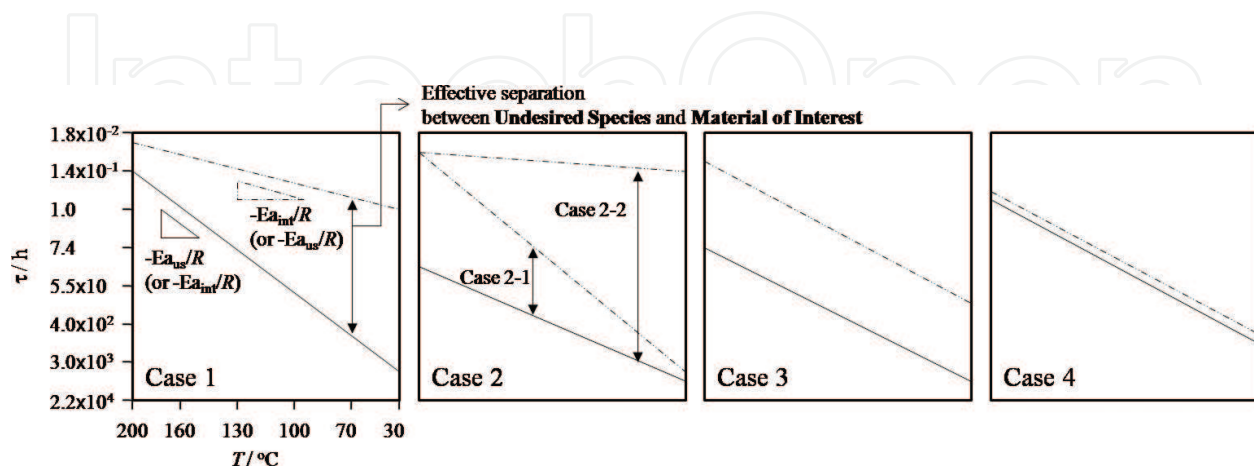


Figure 8. Various cases between the undesired species and the material of interest in the $\tau - T$ diagram (Um, 2012) [18].

CeO₂:

$$k = 1.43 \times 10^8 e^{-14800/T} C^{6.54} \quad (29)$$

Al₂O₃:

$$k = 1.23 \times 10^{13} e^{-15500/T} C^{0.41} \quad (30)$$

Putting the calculated $k'_5 = 1.43 \times 10^8$ (CeO₂) and $k'_5 = 1.23 \times 10^{13}$ (Al₂O₃), $\frac{E_{a_{int}}}{R} = 14800$ (CeO₂) and $\frac{E_{a_{us}}}{R} = 15500$ (Al₂O₃), and $m_{int} = 6.54$ (CeO₂) and $m_{us} = 0.41$ (Al₂O₃) into Eqs. (25) and (26), the expressions between $\ln k$ and $1/T$ at various acid concentrations (C) can be obtained as follows.

$(1/T) \times 10^3$ from 2.1 to 3.1, here C is 8:

CeO₂:

$$\ln k = -14800/T + 32.4 \quad (31)$$

Al₂O₃:

$$\ln k = -15500/T + 31.0 \quad (32)$$

Here C is 10:

CeO₂:

$$\ln k = -14800/T + 33.8 \quad (33)$$

Al₂O₃:

$$\ln k = -15500/T + 31.1 \quad (34)$$

Here C is 12:

CeO₂:

$$\ln k = -\frac{14800}{T} + 35.0 \quad (35)$$

Al₂O₃:

$$\ln k = -15500/T + 31.2 \quad (36)$$

Here C is 14:

CeO₂:

$$\ln k = -14800/T + 36.0 \quad (37)$$

Al_2O_3 :

$$\ln k = -15500/T + 31.2 \quad (38)$$

The revised $\tau - T$ diagram for a $\text{CeO}_2\text{-Al}_2\text{O}_3\text{-H}_2\text{SO}_4\text{-H}_2\text{O}$ system can then be constructed as shown in **Figure 9** using the expressions given previously; the boiling points of $\text{H}_2\text{SO}_4\text{-H}_2\text{O}$ solutions at different acid concentrations of 8, 10, 12, and 14 mol/dm³ were calculated using OLI® software. Like Case 3, the two lines of CeO_2 (material of interest) and Al_2O_3 (undesired species) are nearly parallel with a given separation at each acid concentration. Particularly, the difference in τ increases with increasing acid concentration because cerium has a higher sensitivity of acid concentration than Al_2O_3 ; the large acid concentration constant of 6.54 indicates a strong effect of acid concentration on the dissolution rate of CeO_2 , whereas Al_2O_3 (0.41) has less effect on the dissolution rate owing to changing acid concentration.

5.3. Devised $\tau - T$ diagram application to a hydrometallurgical method with acid leaching process

As mentioned in Section 5.2, the devised $\tau - T$ diagram can be used to predict the dissolution behavior between material of interest and undesired species in the leaching process. As an example, Um and Hirato (2013) [14] reporting the recovery of cerium from rare earth polishing powder wastes presented the devised $\tau - T$ diagram application to a hydrometallurgical method with acid leaching process.

As shown in **Figure 10**, this method involved a two-stage leaching process in series with sulfuric acid solution, which was efficient to dissolve the main elements selectively and then

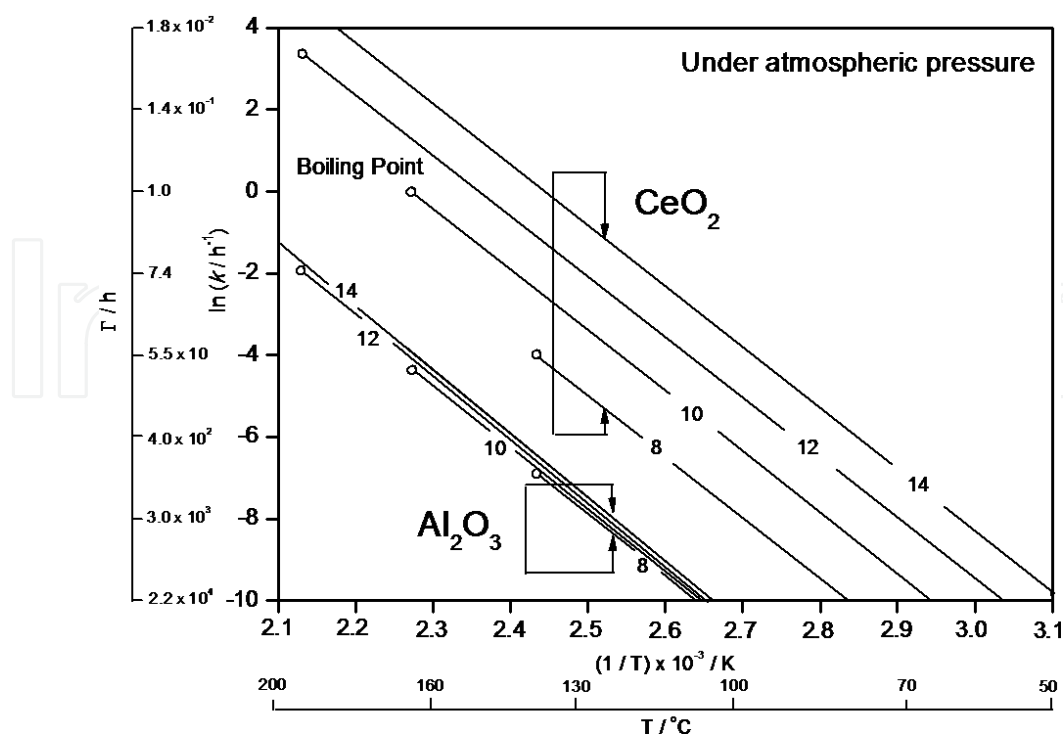


Figure 9. Revised $\tau - T$ diagram for $\text{CeO}_2\text{-Al}_2\text{O}_3\text{-H}_2\text{SO}_4\text{-H}_2\text{O}$ system (Um and Hirato 2013) [14].

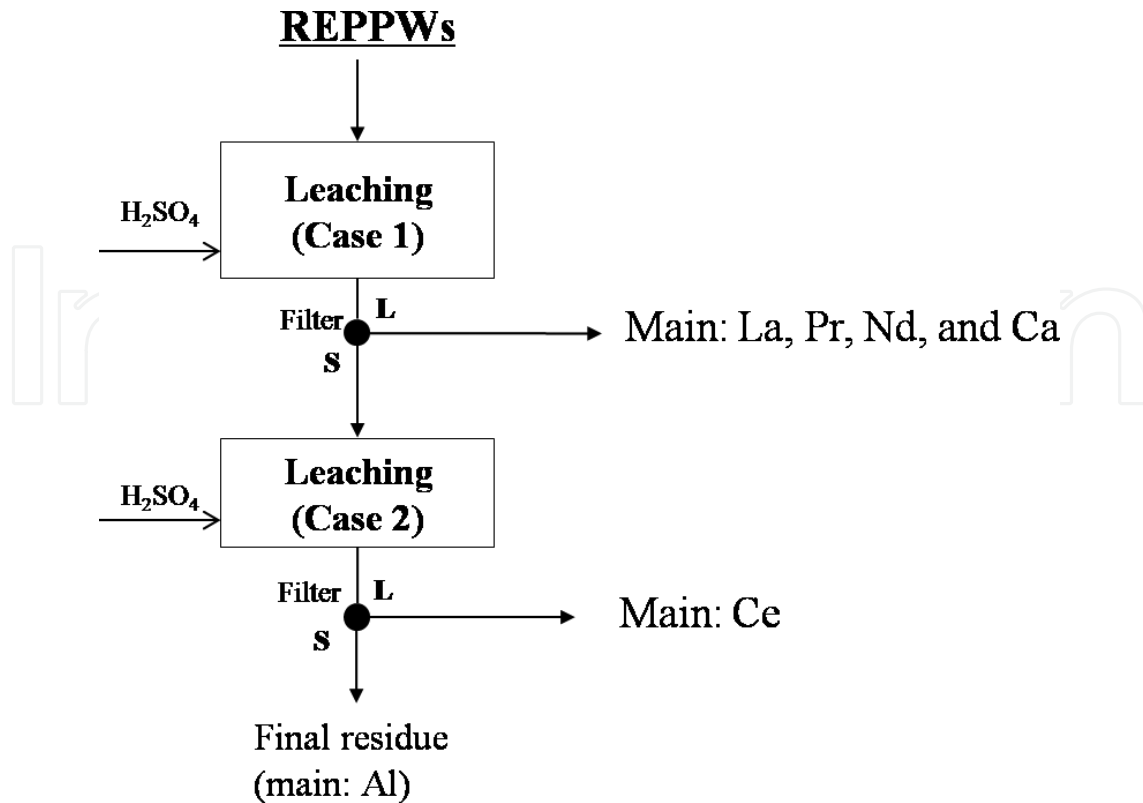


Figure 10. Schematic flow diagram for hydrometallurgical treatment of rare earth polishing powder waste for recovery cerium (Um and Hirato 2013) [14].

to recover cerium. Each dissolution experiment of stage 1 with La_2O_3 , Pr_2O_3 , Nd_2O_3 , and CaO and stage 2 with CeO_2 with CeO_2 and Al_2O_3 by means of two-stage leaching was studied. In particular, after Step 1, CeO_2 can be dissolved leaving Al_2O_3 in a stable solid phase under dissolution conditions calculated using the revised $\tau - T$ diagram for a $\text{CeO}_2\text{-Al}_2\text{O}_3\text{-H}_2\text{SO}_4\text{-H}_2\text{O}$ system shown in **Figure 9**; the increasing difference in τ between cerium and aluminum in the diagram leads CeO_2 to be separated from Al_2O_3 almost completely by leaching.

6. Future plan for technical scale

The perspectives of the studied hydrometallurgical recovery process of REEs from waste for potential chemical engineering applications could be discussed, including the preliminary estimation of energy consumptions and cost. For future plan of technical scale, the various conditions in lab-scale experiment, discussed in each section, including waste composition, reaction temperature, reaction time, chemical reagent, equipment etc, need to be considered as the factor of the preliminary estimation of energy consumptions and cost of the hydrometallurgical process in this study. For example, the reaction temperature and the acid concentration in synthesis of $\text{NaCe}(\text{SO}_4)_2\cdot\text{H}_2\text{O}$ from CeO_2 in $\text{Na}_2\text{SO}_4\text{-H}_2\text{SO}_4\text{-H}_2\text{O}$ solutions discussed in Section 4.2 and leaching of CeO_2 from the mixture of CeO_2 and Al_2O_3 in $\text{CeO}_2\text{-Al}_2\text{O}_3\text{-H}_2\text{SO}_4\text{-H}_2\text{O}$ solution discussed in Section 5.3 belong to a main factor of energy consumption:

1. On the basis of the temperature effect on the hydrometallurgical process with leaching and synthesis processes connecting with the reaction time, an appropriate control condition between temperature and reaction time on recovery method of REEs from waste will lead to the saving of energy consumption.
2. The control of acid concentration on the leaching process connecting with the reaction time and the precipitate after leaching (mentioned in Section 4.1) efforts toward the simplification of total process, and it will lead to savings in cost consumption.
3. The *in situ* recycling of acid solution, reaction reagent, etc. using in the hydrometallurgical process will be a cost-saving method.
4. Cheap and commercial available polyvinyl of polyvinyl chloride and polypropylene is an excellent material for recovery equipments of REEs, especially both reactor and filter in an acidic medium.

However, one concern is the energy- and cost-effectiveness of the hydrometallurgical recovery process of REEs from waste because, as mentioned in Section 1, this depending on the rare earth price in world market being unstable. For example, China monopolizes the supply chain for rare earth, and there have been growing concerns over limited supply in other countries; many countries' trading companies and manufactures have been taking the initiative to secure other sources of rare metals. As such, we have to recognize the strategy to secure a stable supply of rare metals. Indeed, the race to obtain rare metals has started. Therefore, it is necessary to find more affordable alternatives to ensure the sustainability of the energy- and cost-effectiveness in the future plan for technical scale.

7. Conclusion

Hydrometallurgical processes, which mainly include leaching, solvent extraction, ion exchange and precipitation, are widely applied in many fields ranging from environmentally friendly methods for the treatment of raw materials to recovery of material of interest from waste. In the recovery field, the prominent application of leaching process among the hydrometallurgical processes can be the method to improve or to help the effective recovery.

In this chapter, we introduced the main application of acid leaching as a hydrometallurgical method needed in order to recovery rare earth elements (REEs) from waste containing rare earths because the leaching behavior of rare earth on acid solution can be the key to effective recovery as well as advantages including lower capital and lower operating costs. For purification of REEs, the synthesis method of target rare earth during acid leaching was also discussed; for example, the synthesis of rare earths and sodium double sulfate ($\text{NaCe}(\text{SO}_4)_2 \cdot \text{H}_2\text{O}$) is one of the simpler purification methods

In addition, the devised $\tau - T$ diagram application to the hydrometallurgical method for selective acid leaching was discussed. The devised $\tau - T$ diagram can be used to predict the dissolution behavior between REEs and undesired species in the leaching process using the

results of leaching kinetics of rare earths in acid solutions. Therefore, this application can lead to advanced means of obtaining more effective recovery of REEs.

Author details

Namil Um

Address all correspondence to: inhaking96@hotmail.com

National Institute of Environmental Research, Incheon, Korea

References

- [1] Wubbeke J. Rare earth elements in China: Policies and narratives of reinventing an industry. *Resources Policy*. 2013;**38**:384–394. DOI: 10.1016/j.resourpol.2013.05.005
- [2] Baldi L, Peri M, Vandone D. Clean energy industries and rare earth materials: Economic and financial issues. *Energy Policy*. 2014;**66**:53–61. DOI: 10.1016/j.enpol.2013.10.067
- [3] Tao X, Huiqing P. Formation cause, composition analysis and comprehensive utilization of rare earth solid wastes. *Journal of Rare Earths*. 2009;**27**:1096–1102. DOI: 10.1016/S1002-0721(08)60394-4
- [4] Folgueras MB, Alonso M, Fernandez FJ. Coal and sewage sludge ashes as sources of rare earth elements. *Fuel*. 2017;**192**:128–139. DOI: 10.1016/j.fuel.2016.12.019
- [5] Funari V, Bokhari SNHB, Meisel T, Braga R. The rare earth elements in municipal solid waste incinerators ash and promising tools for their prospecting. *Journal of Hazardous Materials*. 2016;**301**:471–479. DOI: 10.1016/j.jhazmat.2015.09.015
- [6] Reed DW, Fujita Y, Daubaras DL, Jiao Y, Thompson VS. Bioleaching of rare earth elements from waste phosphors and cracking catalysts. *Hydrometallurgy*. 2016;**166**:34–40. DOI: 10.1016/j.hydromet.2016.08.006
- [7] Tunsu C, Petranikova M, Ekberg C, Retegan T. A hydrometallurgical process for the recovery of rare earth elements from fluorescent lamp waste fractions. *Separation and Purification Technology*. 2016;**161**:172–186. DOI: 10.1016/j.seppur.2016.01.048
- [8] Yang X, Zhang J, Fang X. Rare earth element recycling from waste nickel-metal hydride batteries. *Journal of Hazardous Materials*. 2014;**279**:384–388. DOI: 10.1016/j.hazmat.2014.07.027
- [9] Doyle FM. Teaching and learning environmental hydrometallurgy. *Hydrometallurgy*. 2005;**79**:1–14. DOI: 10.1016/j.hydromet.2004.10.022
- [10] Jha MK, Kumari A, Panda R, Kumar JR, Yoo K, Lee JY. Review on hydrometallurgical recovery of rare earth metals. *Hydrometallurgy*. 2016;**165**:2–26. DOI: 10.1016/j.hydromet.2016.01.035

- [11] Kim E, Osseo-Asare K. Aqueous stability of thorium and rare earth metals in monazite hydrometallurgy: Eh-pH diagrams for the systems Th-, Ce-, La-, Nd- (PO₄)-(SO₄)-H₂O at 25°C. *Hydrometallurgy*. 2012;**113–114**:67–78. DOI: 10.1016/j.hydromet.2011.12.007
- [12] Scott A, Hayes PY, Thomas JO, Matthew JO, James OS. The phase stability of cerium species in aqueous systems: I. E-pH diagram for the Ce-HClO₄-H₂O system. *Journal of the Electrochemical Society*. 2002;**149**:C623–C630. DOI: 10.1149/1.1516775
- [13] Um N, Hirato T. Precipitation of cerium sulphate converted from cerium oxide in sulphuric acid solutions and the conversion kinetics. *Materials Transactions*. 2012;**11**:1986–1991. DOI: 10.2320/matertrans.M-M2012826
- [14] Um N, Hirato T. Dissolution behavior of La₂O₃, Pr₂O₃, Nd₂O₃, CaO and Al₂O₃ in sulfuric acid solutions and study of cerium recovery from rare earth polishing powder waste via two-stage sulfuric acid leaching. *Materials Transactions*. 2013;**54**:713–719. DOI: 10.2320/matertrans.M-M2013802
- [15] Um N, Hirato T. Conversion kinetics of cerium oxide into sodium cerium sulphate in Na₂SO₄-H₂SO₄-H₂O solutions. *Materials Transactions*. 2012;**11**:1992–1996. DOI: 10.2320/matertrans.M-M2012827
- [16] Um N, Hirato T. A hydrometallurgical method of energy saving type for separation of rare earth elements from rare earth polishing powder wastes with middle fraction of ceria. *Journal of Rare Earths*. 2016;**34**:536–542. DOI: 10.1016/S1002-0721(16)60059-5
- [17] Wadsworth ME, Miller JD. Hydrometallurgical processes. In: Sohn HY, Wadsworth ME, editors. *Rate Processes of Extractive Metallurgy*. New York: Springer; 1979. pp. 133–244. DOI: 10.1007/978-1-4684-9117-3
- [18] Um N. Development of recovery process of rare metals from various resources including rare metal waste by hydrometallurgical process [thesis]. Kyoto: Kyoto University; 2012

IntechOpen